



Structural, photophysical and theoretical studies of two dodecachlorinated porphyrins

Hongshan He^{a,*}, Yihan Zhong^a, Liping Si^{a,b}, Andrew Sykes^b

^a Center for Advanced Photovoltaics, Department of Electrical Engineering and Computer Science, South Dakota State University, SD 57007, USA

^b Department of Chemistry, University of South Dakota, Vermillion, SD 56069, USA

ARTICLE INFO

Article history:

Received 10 March 2011

Received in revised form 3 August 2011

Accepted 3 August 2011

Available online 22 August 2011

Keywords:

Porphyrin

Nickel

Chlorination

Halogenation

Single-crystal structure

ABSTRACT

Two dodecachlorinated porphyrins, 2,3,7,8,12,13,17,18-octachloro-5,10,15,20-tetra(4-chlorophenyl)porphyrin free base (TC₁₂PPH₂) and its nickel compound (TC₁₂PPNi), have been synthesized. Single-crystal X-ray diffraction analysis shows that porphyrin rings are heavily distorted and exhibit saddled conformations. The Soret and Q bands of two compounds are red-shifted compared to their non-chlorinated counterparts. Theoretical calculations reveal that the optical band gap of TC₁₂PPH₂ is reduced, whereas that of TC₁₂PPNi remains almost the same as to its non-chlorinated nickel compound due to the concurrent lowering of HOMO and LUMO energy levels. The frontier molecular orbitals are degenerated due to the decrease of symmetry of the molecules.

© 2011 Elsevier B.V. All rights reserved.

1. Introduction

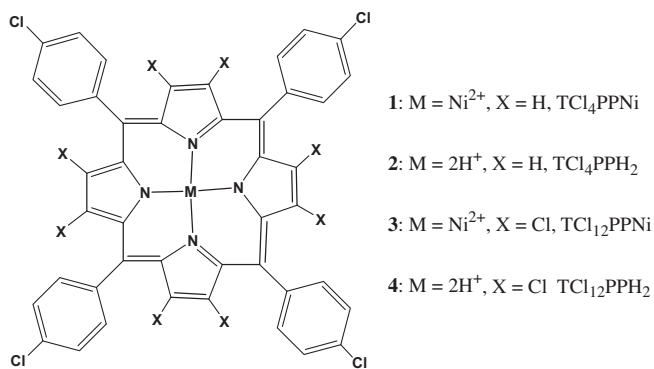
Halogenated porphyrins have strong absorption in the UV–Vis region, moderate yield of triplet state, and strong binding capability to form complexes with different metal ions. They exhibit strong thermal and chemical stability and have been investigated as catalysts for oxygenation of hydrocarbons [1]. The halogenated porphyrins are also attractive chromophores for the sensitization of the near-infrared emission of lanthanide ions. It is well known that the overtones of C–H bond vibration match the frequencies of the NIR emission [2]. When the percentage of C–H bonds in porphyrin is high, part of energy in the excited state dissipates into surrounding environment through overtones instead of giving emission through the relaxation to the ground state. This weakens the emission intensity significantly. When the porphyrin is halogenated, the C–H bonds are replaced by C–X (X = F, Cl, and Br) bonds. As the vibration frequency of C–X bond falls out of overtones of C–H vibration, it will not quench the NIR emission [3,4]. In addition, the halogen atom can also exert “heavy atom” effect on the turnover of electron spinning in the molecular orbital for high yields of triplet state of porphyrin, which is critical for efficient sensitization of NIR emission of lanthanide ions [5]. The halogenated porphyrins are also good candidates for efficient harvesting of sunlight [6]. The halogenated porphyrins usually exhibit broader

absorption capability; therefore they can be used as broadband absorbers for sunlight-harvesting in organic solar cells, such as dye-sensitized solar cells. However, research in these two directions is scarce. The detailed structural, photophysical and theoretical studies of halogenated porphyrins will be very help for these applications.

The halogenation of porphyrin often occurs at its β-pyrrolic positions. The halogenation can be achieved by using different halogenation agents, such as NBS, bromine liquid, and NCS. Eight β-pyrrolic positions, as well as phenyl groups in *meso* positions, can be halogenated using these methods. One obvious result from halogenation is the distortion of ring structure [7–12]. The non-halogenated porphyrin ring is usually planar. When part or all of pyrrolic protons are substituted by halogen atoms, the porphyrin ring is distorted. In 1997, Spyroulias et al. reported [13] the crystal structure of an octabromotetraphenylporphyrin and found the porphyrin ring had a saddled conformation. In 2002, these authors reported [6] the crystal structure of octachlorotetraphenylporphyrin nickel compound and a similar structural conformation was also observed. However, the structure and photophysical properties of porphyrins that are halogenated by more than eight chlorine atoms are rarely reported. In this paper, we described the structure, photophysical properties and theoretical calculations of two dodecachlorinated porphyrins as shown in Scheme 1. It is expected that these results will provide some structural and theoretical insights for the sensitization of lanthanide emission and harvesting of sunlight.

* Corresponding author. Tel.: +1 605 6886962; fax: +1 605 6884401.

E-mail address: Hongshan.he@sdsatet.edu (H. He).



Scheme 1. Structure of chlorinated porphyrins.

2. Experimental

2.1. General

4-Chlorophenylbenzaldehyde was purchased from Sigma–Aldrich. Pyrrole was obtained from Acros and distilled twice prior to use. Other chemicals were used directly without further treatment. Elemental analysis (C, H, and N) were performed on a commercial CHN analyzer. FT-IR spectra were obtained on a Nicolet 6700 spectrometer. Tetrakis(4-chlorophenyl)porphyrin (TCl₄PPH₂) was synthesized according to the literature method [14]. Its nickel complex (TCl₄PPNi) was synthesized by the reaction between TCl₄PPH₂ and nickel acetate in DMF. UV–Vis absorption spectra were recorded on an HP Agilent 5439 spectrophotometer using 1.0 cm quartz cell. Steady-state luminescence spectra were obtained on an FS920 fluorescence spectrometer (Edinburgh Instrument, Inc., UK) with an arc lamp (Xe900) as light source and Hamamatsu R928P as detector. Fluorescence decay curves were acquired on LifeSpec II spectrometer (Edinburgh Instrument, Inc., UK) using time-correlated single photon counting technique. The intensities were monitored using a Hamamatsu H5773-02 detector. A pulse diode laser (EPL-375, Edinburgh Instrument, Inc., UK) with excitation wavelength at 375 nm was used as light source and lifetimes were obtained by exponential fitting of deconvoluted data.

2.2. Synthesis of TCl₁₂PPNi

To a solution of TCl₄PPNi (0.42 g, 0.53 mmol) in 1,2-dichlorobenzene (30 mL) was added NCS (0.83 g, 133 mmol). The solution was refluxed under N₂ for 2 h. Then solvent was removed under vacuum. The solid was dissolved in chloroform, loaded on a silica gel column, and eluted with chloroform. The second band was collected as TCl₁₂PPNi. The compound was precipitated out from CHCl₃/MeOH. The final shining green crystals were obtained after slow evaporation of solvents in CHCl₃/MeOH (v:v: 1:3) at room temperature for three weeks. The crystals were very stable in the air and used directly for analysis. Yield: 0.42 g. *Anal.* Calc. for C₄₄H₁₆Cl₁₂N₄Ni·2CH₃OH·HCl: C, 46.61; H, 2.13; N, 4.73. Found: C, 46.35; H, 2.24; N, 4.87%.

2.3. Synthesis of TCl₁₂PPH₂

To a solution of TCl₁₂PPNi (0.40 g, 0.53 mmol) in dichloromethane (100 mL) at room temperature was added concentrated H₂SO₄ (30 mL) under vigorous magnetic stirring. The mixture was stirred for 4 h, and then water (100 mL) was added slowly while the flask was kept in an ice bath. The organic phase was washed by water several times to remove acid. The organic solvent was then reduced

to ~5 mL on a rotary evaporator and loaded on a column (silica gel) for purification. The major band was collected. After removing all solvent, the compound was re-dissolved in CHCl₃/MeOH (v:v: 1:3) solution and kept at room temperature. The shining green crystals were obtained in two weeks after slow evaporation of solvent. The crystals were very stable in the air and were used directly for analysis. Yield: 3.6 g. *Anal.* Calc. for C₄₄H₁₆Cl₁₂N₄·3CH₃OH·2H₂O·HCl: C, 47.89; H, 2.82; N, 4.75. Found: C, 47.72; H, 2.68; N, 4.65%.

2.4. Single-crystal X-ray diffraction analysis

The crystals were mounted on glass fiber for data collection. Diffraction measurements were made on a CCD-based commercial X-ray diffractometer using Mo K α radiation ($\lambda = 0.71073$ Å). The frames were collected at ambient temperature with a scan width 0.3° in ω and integrated with the Bruker SAINT software [15] package using the narrow-frame integration algorithm. The unit cell was determined and refined by least squares upon the refinement of XYZ-centeroids of reflections above 20 $\theta(I)$. The data were corrected for absorption using SADABS program [16]. The structures were refined on F^2 using the SHELX97 [17]. The structural parameters were listed in Table 1.

2.5. Density functional theory calculations

Theoretical calculations were performed at a density functional theory (DFT) level using GAUSSIAN 09 software [18]. The initial input structures were built using structure builder tools. The ground state geometry was optimized using 6-31G as basis set and B3LYP as functional in vacuum. All other parameters were default set. No negative frequency was found in the final optimized structures. The time-dependent (TD) DFT calculations were carried out using 6-31G as basis set and B3LYP as functional in dichloromethane. The continuum (CPCM) model was used for mimicking the solvent effect.

Table 1

X-ray crystallographic data for TCl₁₂PPNi and TCl₁₂PPH₂.

	TCl ₁₂ PPNi	TCl ₁₂ PPH ₂
Empirical formula	C ₄₆ H ₂₄ Cl ₁₃ N ₄ O ₂ Ni	C ₄₈ H ₃₃ Cl ₁₃ N ₄ O ₇
Formula weight	1184.25	1238.7
<i>T</i> (K)	293(2)	293(2)
Wavelength (Å)	0.71073	0.71073
Crystal system	triclinic	orthorhombic
Space group	<i>P</i> $\bar{1}$	<i>Pnma</i>
Cell dimensions		
	10.2004(11)	17.712(3)
	15.7149(17)	27.969(4)
	16.4728(18)	10.1333(15)
	113.4690(10)	90
	93.3900(10)	90
	104.1000(10)	90
<i>Z</i>	2	4
ρ_{calc} (g cm ⁻³)	1.701	1.639
μ (Mo K α) (mm ⁻¹)	1.217	0.772
<i>F</i> (0 0 0)	1186	2504
θ Range for data collected (°)	2.09–25.00	2.14–25.90
Reflections collected/independent	22 681/8092	49 157/4970
Data/restraints/parameters	8092/0/600	4970/0/337
Goodness-of-fit (GOF) on F^2	1.156	1.051
Final <i>R</i> indices [$I > 2\sigma(I)$]	<i>R</i> ₁ = 0.0753, <i>wR</i> ₂ = 0.2012	<i>R</i> ₁ = 0.0742, <i>wR</i> ₂ = 0.2161
<i>R</i> indices (all data)	<i>R</i> ₁ = 0.098, <i>wR</i> ₂ = 0.2128	<i>R</i> ₁ = 0.0939, <i>wR</i> ₂ = 0.2362

3. Results and discussion

3.1. Synthesis and characterization

The nickel(II) complex ($\text{TCI}_{12}\text{PPNi}$) was obtained by direct reaction between 5,10,15,20-tetra(4-chlorophenyl)porphyrinatonickel(II) (TCI_4PPNi) and NCS in 1,2-dichlorobenzene with high yield. The free base ($\text{TCI}_{12}\text{PPH}_2$) was obtained by demetallation of $\text{TCI}_{12}\text{PPNi}$ in the presence of H_2SO_4 in dichloromethane. Both compounds were purified on column (silica gel) using chloroform as elute. When the compounds precipitated out from chloroform solution using methanol, they were dark purple powder; however, when they crystallized from dichloromethane/methanol solution after slow evaporation of solvent, the color of obtained crystals was dark green. The solubility of two compounds in chloroform and dichloromethane is relatively low compared to non-chlorinated counterparts. When they are dissolved in chloroform, the color of $\text{TCI}_{12}\text{PPNi}$ solution is reddish, whereas that of $\text{TCI}_{12}\text{PPH}_2$ is green. It should be noted that crystals of two compounds are very stable in the air. No visible change was observed for two years. In this study, we use those crystals directly for structure characterization including single-crystal X-ray diffraction analysis and photophysical measurements.

The FT-IR spectra of $\text{TCI}_{12}\text{PPNi}$ and $\text{TCI}_{12}\text{PPH}_2$ are very similar to each other. The C=N vibrations are 1450 cm^{-1} for $\text{TCI}_{12}\text{PPH}_2$ and 1479 cm^{-1} for $\text{TCI}_{12}\text{PPNi}$, respectively. The C=C vibrations are 1587 and 1592 cm^{-1} for free base and Ni compound, respectively. For free base a broad peak at 3450 cm^{-1} was observed for N-H vibration from porphyrin ring. In addition, two peaks at 2930 and 2881 cm^{-1} , corresponding to the C-H vibration of phenyl groups were also observed for both compounds. The peaks between 500 and 1200 cm^{-1} are very similar to those of TCI_4PPH_2 , as shown in Fig. 1. After chlorination, the number of vibration peaks reduced.

3.2. Single-crystal structure

Fig. 2 shows the ORTEP diagram of $\text{TCI}_{12}\text{PPNi}$ with 50% thermal ellipsoid probability. There are twelve Cl atoms in each molecule: four in the *para* positions of phenyl groups and eight in the β -pyrrolic positions. The Ni^{2+} is located in the center of the porphyrin ring. It is coordinated by four N atoms from porphyrin ring and one O atom from methanol solvate. The ring structure of $\text{TCI}_{12}\text{PPNi}$ is distorted dramatically. One pair of pyrrole groups on the opposite positions of the porphyrin ring bend to one direction; whereas

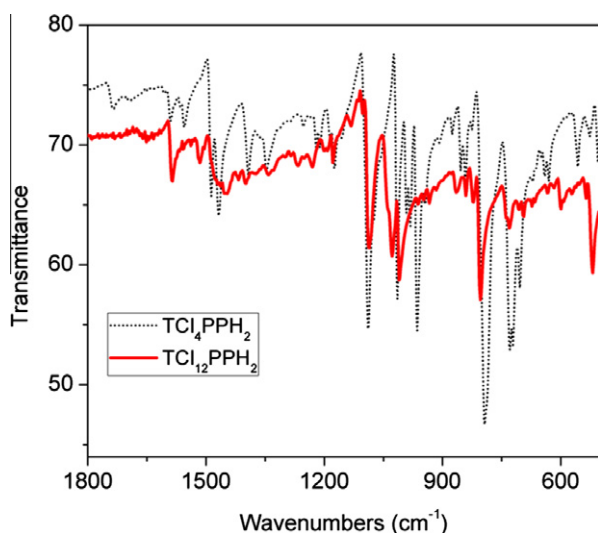


Fig. 1. FT-IR spectra of TCI_4PPH_2 and $\text{TCI}_{12}\text{PPH}_2$.

another pair goes to opposite direction. The torsion angles between the mean plane of pyrroles are $44.55(38)^\circ$ and $33.23(38)^\circ$ for the pair $P1/P3$ and the pair $P2/P4$, respectively. These are significantly larger than regular porphyrins. Surprisingly the four N atoms almost fall into one plane with RMS deviation 0.0556 . Two methanol solvates and two HCl molecules were found in each asymmetric unit. The methanol comes from the solvent during the crystallization and purification. The HCl may come from the cleavage of C-Cl bonds during the chlorination.

Fig. 3 shows the ORTEP diagram of $\text{TCI}_{12}\text{PPH}_2$. The overall structural feature is very similar to its nickel compound. Two pairs of pyrrole groups, pair $P1/P3$ and pair $P2/P4$, also bend in a similar fashion as observed in compound $\text{TCI}_{12}\text{PPNi}$. The torsion angles between two pyrrole pairs are $72.64(29)^\circ$ and $76.83(18)^\circ$ for $P1/P3$ and $P2/P4$, respectively. The pyrrole rings are bent more heavily in $\text{TCI}_{12}\text{PPH}_2$ than in $\text{TCI}_{12}\text{PPNi}$. The four N atoms also fall into one plane with RMS deviation 0.0687 . It was found that one water molecule was trapped inside the porphyrin ring. It forms hydrogen bond with one methanol molecule. It is worth mentioning that crystals of $\text{TCI}_{12}\text{PPH}_2$ exhibit very good external shape; however the quality of refined structure is not as good as $\text{TCI}_{12}\text{PPNi}$. We also collected data for other two crystals from same batch; however the overall quantity of the structure was not improved. There is one strong peak in the center of the porphyrin, which was modeled as O atom during the refinement to achieve best result. Nevertheless, porphyrin ring and phenyl groups including all chlorine atoms are well defined.

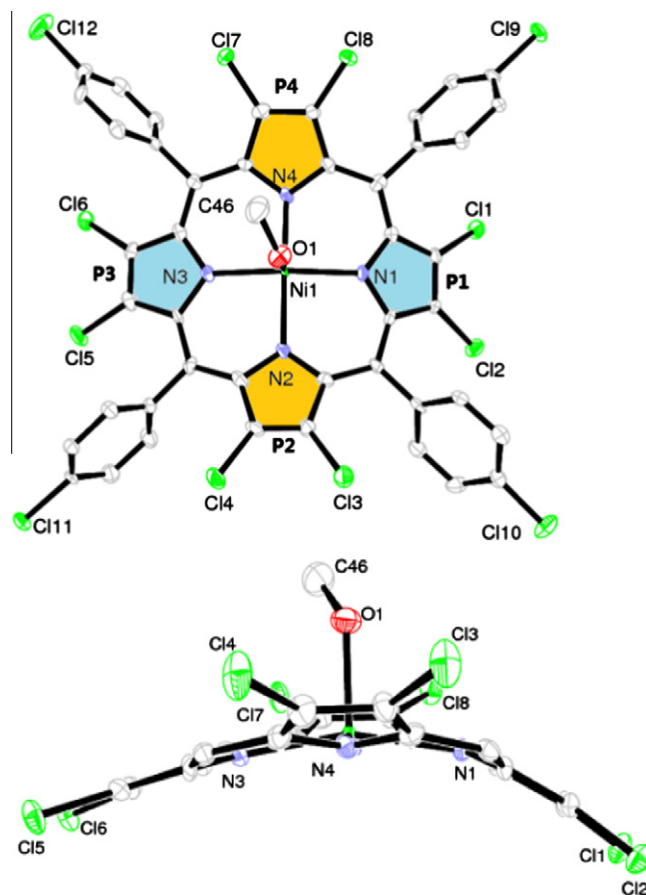


Fig. 2. ORTEP diagrams of $\text{TCI}_{12}\text{PPNi}$ with 50% thermal stability. Hydrogen atoms were omitted for clarity. Top: top view of the structure. Two pairs of pyrrole groups ($P1/P3$ and $P2/P4$) were color-coded; bottom: side view of core structure (four phenyl groups were omitted for clarity). Selected bond lengths (Å): $\text{N1-Ni1} = 2.081(7)$, $\text{N2-Ni1} = 2.085(7)$, $\text{N3-Ni1} = 2.060(7)$, $\text{N4-Ni1} = 2.077(7)$, $\text{O1-Ni1} = 2.087(6)$.

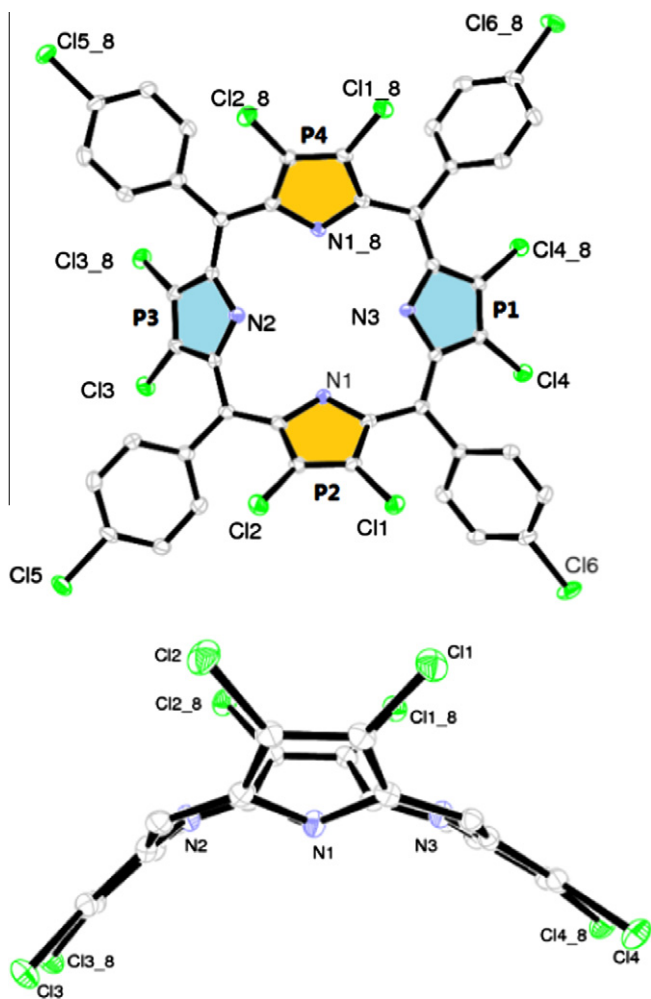


Fig. 3. ORTEP diagrams of $\text{TCl}_{12}\text{PPH}_2$ with 50% thermal ellipsoid probability. Hydrogen atoms were omitted for clarity. Top: top view of the structure. Two pairs of pyrrole groups (P1 and P3, P2 and P4) were color-coded; bottom: side view of core structure (four phenyl groups were omitted for clarity).

3.3. Photophysical properties

The absorption spectra of two porphyrins in dichloromethane are shown in Fig. 4. The solution of nickel porphyrin was reddish, whereas solution of free porphyrin was green. Compared to non-halogenated porphyrins the Soret bands of free porphyrin and chlorinated porphyrin are red-shifted to 439 and 453 nm, respectively. In the Q band region, one peak at 555 nm and a shoulder at 575 nm were observed for nickel compound, whereas three peaks at 555, 598 and 728 nm were observed for free base. These peaks are consistent with the literature report on TCl_8PPH_2 and TCl_8PPNi compounds, where only eight β -pyrrolic positions were chlorinated [6]. The addition of four Cl atoms on the *para*-position of phenyl groups did not exert significant influence on the absorption. For free porphyrin a shoulder at 486 nm was also observed, which came from the deprotonated porphyrin. When one drop of pyridine was added to the CH_2Cl_2 solution of $\text{TCl}_{12}\text{PPH}_2$, peak intensity at 486 nm was increased. This is consistent with the crystal structure, in which a water molecule is captured inside the porphyrin core with NH partially deprotonated.

The excitation and emission spectra of free base is shown in Fig. 5. A weak peak centered at 787 nm was observed. The excitation spectrum is consistent with absorption spectrum, indicating the single pathway of emission spectrum. As large as ~ 59

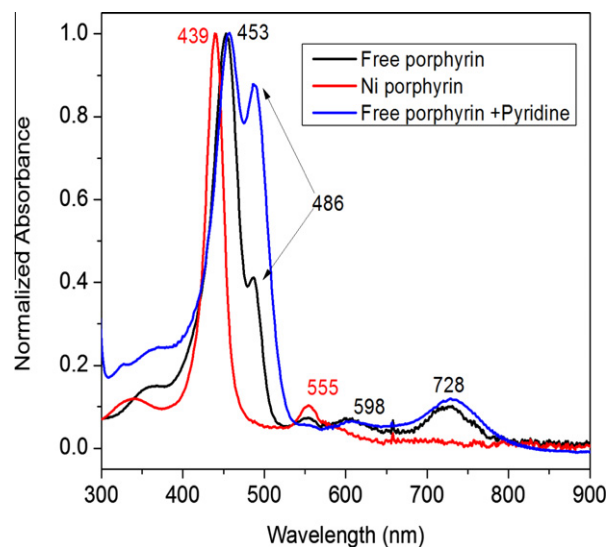


Fig. 4. Absorption spectra of nickel porphyrin $\text{TCl}_{12}\text{PPNi}$ (red) and free base $\text{TCl}_{12}\text{PPH}_2$ (black and blue) in dichloromethane at room temperature. The absorbance was normalized for comparison. The absorption was normalized at Soret peaks. (For interpretation of the references in color in this figure legend, the reader is referred to the web version of this article.)

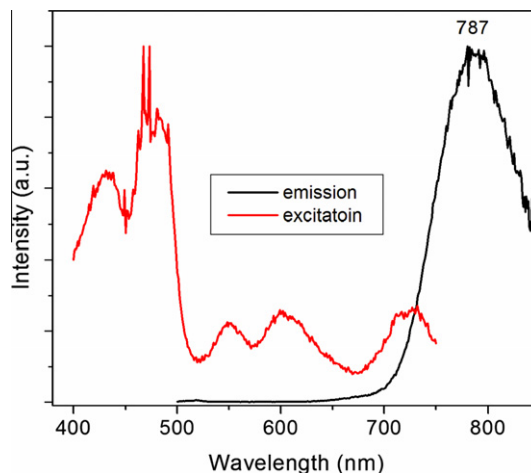


Fig. 5. Emission and excitation spectra of free base $\text{TCl}_{12}\text{PPH}_2$ in dichloromethane at room temperature. The excitation wavelength was 450 nm. The excitation was monitored at 787 nm.

Stokes shift was observed. This indicated that lowest emission state lowered significantly compared to non-halogenated porphyrin due to structural distortion. The decay profile of emission at 787 nm was shown in Fig. 6. The deconvoluted curve fits well single exponentially, resulting a decay lifetime of 0.27 ns. This is significantly lower than those from non-halogenated porphyrins, which are usually in several ns. This is probably due to the vibronic quenching effect from solvent due to this long wavelength emission in the near-infrared region. No fluorescence was observed for nickel porphyrin.

3.4. Theoretical calculations

To further reveal the effect of halogenations on the photophysical properties, the density functional theory calculations were carried out. The geometry-optimized structure of $\text{TCl}_{12}\text{PPNi}$ exhibited similar bond lengths and bond angles to its single-crystal structure,

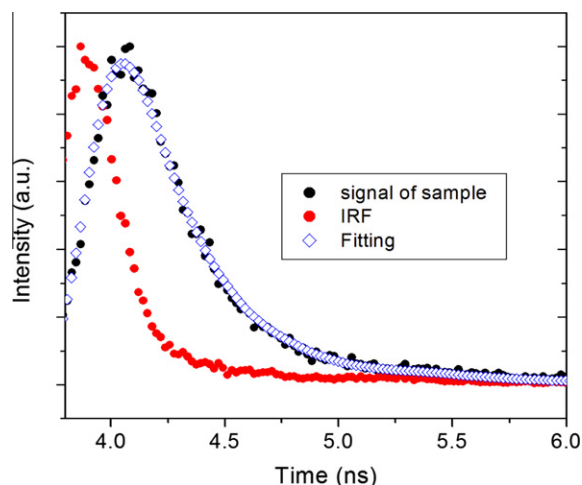


Fig. 6. Fluorescence decay of compound free base $\text{TCl}_{12}\text{PPH}_2$ in dichloromethane at room temperature. The excitation wavelength was 375 nm. The decay was monitored at 787 nm.

indicating the effectiveness of functional and basis sets used for calculations. For comparison purpose the calculations were also performed on TCl_4PPNi and TCl_4PPH_2 without chlorination in the β -pyrrole positions. The electron density profiles of frontier orbitals are shown in Fig. 7, both showing very similar electron distribution to their non-halogenated counterparts, respectively. It was found that the band gap (energy difference between LUMO and HOMO levels) of free porphyrin $\text{TCl}_{12}\text{PPH}_2$ was quite small compared non-chlorinated porphyrin TCl_4PPH_2 , leading to its absorption in the near infrared region, as shown in Table 2. The decrease mainly comes from the lowering of LUMO (-2.6939 eV in TCl_4PPH_2 to -3.5647 eV in $\text{TCl}_{12}\text{PPH}_2$). The HOMO was also lowered compared to that in TCl_4PPH_2 , but not significant compared to LUMO. Surprisingly we found that both HOMO and LUMO of nickel porphyrin $\text{TCl}_{12}\text{PPNi}$ were lowered in the same magnitude, leading to very close band gap compared to non-chlorinated nickel porphyrin TCl_4PPNi . This explains why compound $\text{TCl}_{12}\text{PPNi}$ does not exhibit absorption in the near-infrared region.

Table 2

The HOMO and LUMO energy levels of four porphyrins from calculations.

Porphyrin	HOMO (eV)	LUMO (eV)	HOMO–LUMO gap (eV)
TCl_4PPH_2	-5.5512	-2.8300	2.7212
TCl_4PPNi	-5.6328	-2.6939	2.9388
$\text{TCl}_{12}\text{PPH}_2$	-5.8777	-3.5647	2.3130
$\text{TCl}_{12}\text{PPNi}$	-6.1770	-3.3401	2.7755

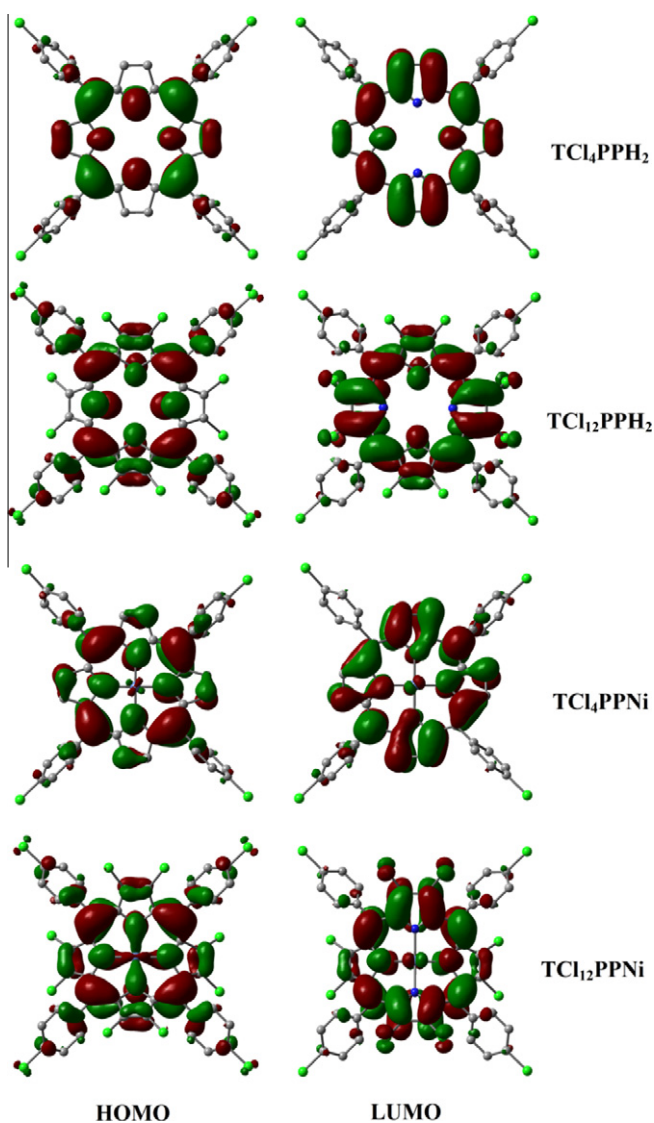


Fig. 7. The electron density profiles of HOMO and LUMO of four porphyrins.

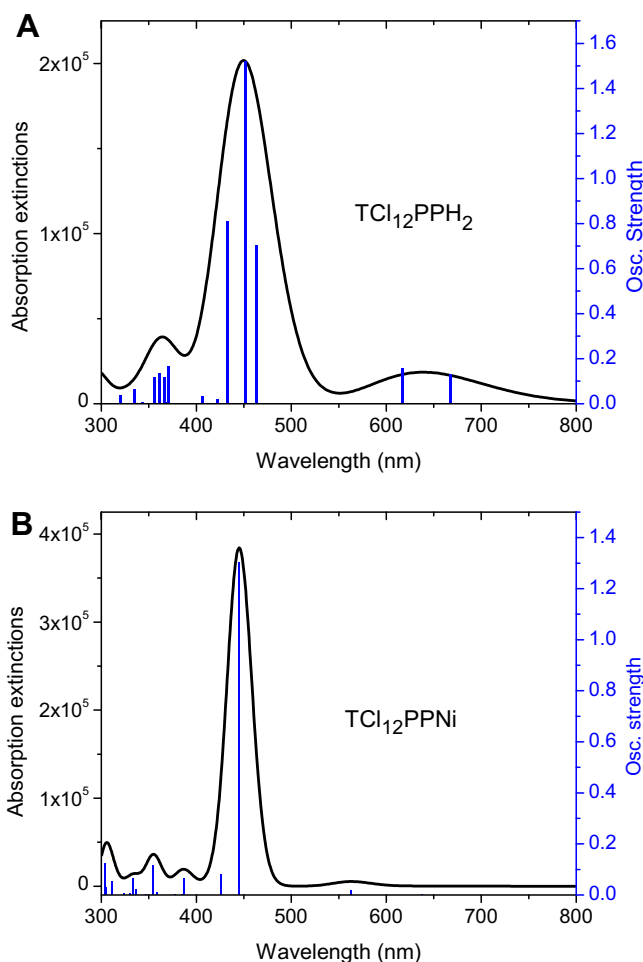


Fig. 8. The calculated absorption spectra of $\text{TCl}_{12}\text{PPH}_2$ (A) and $\text{TCl}_{12}\text{PPNi}$ (B) in dichloromethane and the corresponding oscillation strengths.

Table 3
Major transition of two chlorinated porphyrins and their oscillation strength (*f*).

Porphyrin	Transition	<i>f</i>	Compositions (percentage)	Character
TCl ₁₂ PPH ₂	668.2	0.1328	HOMO–1 → LUMO+1 (19%) HOMO → LUMO (80%)	Singlet
	616.6	0.1552	HOMO–1 → LUMO (25%)	Singlet
	463.2	0.7018	HOMO → LUMO+1 (75%) HOMO–3 → LUMO (25%), HOMO–1 → LUMO+1 (59%) HOMO → LUMO (11%)	Singlet
	451.9	1.5201	HOMO–1 → LUMO (72%) HOMO → LUMO+1 (–24%)	Singlet
	432.4	0.8105	HOMO–3 → LUMO (72%) HOMO–1 → LUMO+1 (16%)	Singlet
	370.3	0.1638	HOMO–8 → LUMO (76%) HOMO–7 → LUMO (21%)	Singlet
TCl ₁₂ PPNi	562.9	0.0181	HOMO–1 → LUMO (19%) HOMO–1 → LUMO+1 (23%) HOMO → LUMO (32%), HOMO → LUMO+1 (–26%)	Singlet
	445.2	1.3008	HOMO–1 → LUMO (54%) HOMO → LUMO+1 (38%)	Singlet
	426.4	0.0809	HOMO–9 → LUMO (–43%) HOMO–4 → LUMO (52%)	Singlet
	386.6	0.0629	HOMO–9 → LUMO (48%) HOMO–5 → LUMO+1 (–10%) HOMO–4 → LUMO (35%)	Singlet

The time-dependent DFT (TD-DFT) calculations were also carried out to reveal how the geometry distortion alters the absorption spectra. The predicted absorption spectra of TCl₁₂PPNi and TCl₁₂PPH₂ are shown in Fig. 8. The predicated Soret bands are 445.1 and 451.9 nm for Ni²⁺ and free base porphyrin, respectively. Both are very close to the experimental data. The predicated Q band for TCl₁₂PPNi is 562 nm, which also matches the measured peak position at 556 nm well. Two Q peaks for TCl₁₂PPH₂ were predicated: 616.6 and 668.1 nm. Both are different from experimental data (554, 598 and 728 nm). This difference could come from the more ruffled structure of free base, which leads to the insufficiency of TD-DFT model for calculation. The geometry optimized structure of TCl₁₂PPH₂ and TCl₁₂PPNi were very similar to each other; however their crystal structures were quite different. The assignments of those peaks and their corresponding oscillation strengths are listed in Table 3, which still can be explained by Gouterman's four orbital models [19] with significant degeneration due to the structure distortion. This model includes two highest occupied orbitals (HOMO and HOMO–1) and two lowest unoccupied orbitals (LUMO and LUMO+1). These results show that frontier orbitals of chlorinated porphyrin are degenerated and gap between orbitals narrowed. As a result, the absorption is red-shifted. More pronounced effect is observed in free base than in nickel compound.

4. Conclusion

The chlorination of eight β-pyrrolic position of porphyrin leads to the distortion of ring structure, resulting saddled conformations. The distortion is more pronounced in free base than in nickel compound. The introduction of additional four chlorine atoms in the *para* position of phenyl group does not exert obvious impact on the porphyrin structure. After chlorination the optical onset red-shifts to the near-infrared region for free base; however, no significant

red-shift is observed for nickel compound. The theoretical calculation reveals that red-shift in the free base comes from significant lowering of LUMO energy level.

Acknowledgements

This material is based upon work supported by the National Science Foundation/EPSCoR (0903804), the State of South Dakota, and Ph.D. program in the Department of Electrical Engineering and Computer Science, SDSU, and South Dakota State University Administration & Research Computing.

Appendix A. Supplementary material

CCDC 812564 and 812565 contain the supplementary crystallographic data for this paper. These data can be obtained free of charge from The Cambridge Crystallographic Data Centre via www.ccdc.cam.ac.uk/data_request/cif. Supplementary data associated with this article can be found, in the online version, at [doi:10.1016/j.ica.2011.08.006](https://doi.org/10.1016/j.ica.2011.08.006).

References

- [1] R. Bonnett, A. Harriman, A.N. Kozyrew, J. Chem. Soc., Perkin Trans. 88 (1992) 763.
- [2] S. Comby, J.-C.G. Bünzli, Lanthanide near-infrared luminescence in molecular probes and devices, in: A. Karl, J. Gschneidner, J.-C.G. Bünzli, V.K. Pecharsky (Eds.), Handbook on the Physics and Chemistry of Rare Earths, vol. 37, Elsevier, 2007, p. 217 (Chapter 235).
- [3] J.-C.G. Bünzli, Chem. Rev. 110 (2010) 2729.
- [4] K.M.L. Taylor-Pashow, J. Della Rocca, R.C. Huxford, W. Lin, Chem. Commun. 46 (2010) 5832.
- [5] E.A. Azenha, A.C. Serra, M. Pineiro, M.M. Pereira, J.S. de Melo, L.G. Arnaut, S.J. Formosinho, A.M. d'A Rocha Gonsalves, Chem. Phys. 280 (2002) 177.
- [6] G.A. Spyroulias, A.P. Despotopoulos, C.P. Raptopoulou, A. Terzis, D. de Montauzon, R. Poilblanc, A.G. Coutsolelos, Inorg. Chem. 41 (2002) 2648.
- [7] P. Bhyrappa, V. Krishnan, Inorg. Chem. 30 (1991) 239.
- [8] R. Pizzoferrato, R. Francini, S. Pietrantonio, R. Paolesse, F. Mandoj, A. Monguzzi, F. Meinardi, J. Phys. Chem. A 114 (2010) 4163.
- [9] M. Pineiro, A.L. Carvalho, M.M. Pereira, A.M. d'A Rocha Gonsalves, L.G. Arnaut, S.J. Formosinho, Chem. Eur. J. 4 (1998) 2299.
- [10] C. Raptopoulou, D. Daphnomili, A. Karamalides, M. Di Vaira, A. Terzis, A.G. Coutsolelos, Polyhedron 23 (2004) 1777.
- [11] J. Leroy, B. Schollhorn, J.-L. Syssa-Magale, K. Boubekeur, P. Palvadeau, J. Fluorine Chem. 125 (2004) 1379.
- [12] W. Su, K. Singh, J. Rogers, J. Slagle, P. Fleitz, Mater. Sci. Eng. B 132 (2006) 12.
- [13] G.A. Spyroulias, A. Despotopoulos, C.P. Raptopoulou, A. Terzis, A.G. Coutsolelos, Chem. Commun. (1997) 783.
- [14] A.D. Adler, F.R. Longo, J.D. Finarelli, J. Goldmacher, J. Assour, I. Korsakoff, J. Org. Chem. 32 (1967) 476.
- [15] SAINT+, Ver. 6.02a, Bruker Analytical X-ray System, Inc., Madison, WI, 1998.
- [16] G.M. Sheldrick, SADABS, Empirical Absorption Correction Program, University of Göttingen, Germany, 1997.
- [17] G.M. Sheldrick, SHELXTLM, Reference Manual, Version 5.1, Madison, WI, 1997.
- [18] M.J. Frisch, G.W. Trucks, H.B. Schlegel, G.E. Scuseria, M.A. Robb, J.R. Cheeseman, G. Scalmani, V. Barone, B. Mennucci, G.A. Petersson, H. Nakatsuji, M. Caricato, X. Li, H.P. Hratchian, A.F. Izmaylov, J. Bloino, G. Zheng, J.L. Sonnenberg, M. Hada, M. Ehara, K. Toyota, R. Fukuda, J. Hasegawa, M. Ishida, T. Nakajima, Y. Honda, O. Kitao, H. Nakai, T. Vreven, J.A. Montgomery Jr., J.E. Peralta, F. Ogliaro, M. Bearpark, J.J. Heyd, E. Brothers, K.N. Kudin, V.N. Staroverov, R. Kobayashi, J. Normand, K. Raghavachari, A. Rendell, J.C. Burant, S.S. Iyengar, J. Tomasi, M. Cossi, N. Rega, J.M. Millam, M. Klene, J.E. Knox, J.B. Cross, V. Bakken, C. Adamo, J. Jaramillo, R. Gomperts, R.E. Stratmann, O. Yazyev, A.J. Austin, R. Cammi, C. Pomelli, J.W. Ochterski, R.L. Martin, K. Morokuma, V.G. Zakrzewski, G.A. Voth, P. Salvador, J.J. Dannenberg, S. Dapprich, A.D. Daniels, Ö. Farkas, J.B. Foresman, J.V. Ortiz, J. Cioslowski, D.J. Fox, GAUSSIAN 09, Revision A.1, Gaussian, Inc., Wallingford, CT, 2009.
- [19] M. Gouterman, C.D. Schumaker, T.S. Srivastava, T. Yonetani, Chem. Phys. Lett. 40 (1976) 456.